INTERSTELLAR ENVIRONMENTS IN THE LARGE MAGELLANIC CLOUD

SUNGEUN KIM
Astronomy & Space Science, Sejong University, 98 Gunjadong, Kwangjin-ku, Seoul, 143-747, Korea
E-mail: skim@arcsec.sejong.ac.kr

ABSTRACT

We present the results of an H I aperture synthesis mosaic of the Large Magellanic Cloud (LMC), made by combining data from 1344 separate pointing centers using the Australia Telescope Compact Array (ATCA) and the Parkes multibeam receiver. The resolution of the mosaiced images is $50''$ (<15 pc, using a distance to the LMC of 55 kpc). This mosaic, with a spatial resolution 15 times higher than that which had been previously obtained, emphasises the turbulent and fractal structure of the ISM on the small scale, resulting from the dynamical feedback of the star formation processes with the ISM. We also have done a widefield panoramic survey of Hα emission from the Magellanic Clouds with an imager mounted on the 16-inch telescope at Siding Spring Observatory. This survey produced Hα images which are equal to the ATCA survey in area coverage and resolution. This survey allows us to produce a continuum-subtracted image of the entire LMC. In contrast with its appearance in the Hα image, the LMC is remarkably symmetric in H I on the largest scales, with the bulk of the H I residing in a disk of diameter $8.°4$ (7.3 kpc) and a spiral structure is clearly seen. The structure of the neutral atomic ISM in the LMC is dominated by H I filaments combined with numerous shells and holes.

Key words : galaxies: ISM—ISM: neutral hydrogen—Magellanic Clouds

I. INTRODUCTION

High resolution H I observations of nearby galaxies allow the study of many aspects of their dynamics, morphology and interstellar physics. Measurement of the vertical H I distribution and velocity dispersion, for example, allows the mass-to-light ratio and dark matter content of galaxy disks to be studied (Olling 1996). The shape of the inner velocity field, using H I as a tracer, can discriminate between different halo models (de Blok et al. 2001). Also, the relationship between H II regions and H I holes says much about the evolution of galaxies and the propagation of star-forming regions (Walter & Brinks 2001).

The LMC, as the nearest gas-rich galaxy to our own, has been the subject of several H I studies (Luks & Rohlfs 1992; McGee & Milton 1966). The advantage of studying the LMC in H I is that it is the nearest galaxy to our own with a distance of 50−55 kpc (Feast 1991), it is presented nearly face-on, and it is a very gas-rich and active star forming galaxy, so that it allows for a detailed study of the structure, dynamics and the interstellar medium of a star-forming galaxy at close range. The early single-dish observations revealed the existence of expanding H I shells in the LMC (Westerlund & Mathewson 1996; McGee & Milton 1966). A very spectacular example of such a shell associated with the major star-forming region Constellation III was described by Dopita, Mathewson, & Ford (1985).

However, its location in the far south means that

high resolution studies had to await the advent of the Australia Telescope Compact Array (ATCA). The advent of ATCA finally allowed us to take full advantage of the aperture synthesis technique in southern hemisphere observations, and our recent high-resolution H I survey of the Large Magellanic Cloud (LMC) revealed that the structure of the neutral atomic interstellar gas to be dominated by numerous shells and holes as well as complex filamentary structure (Kim et al. 1998a). Its huge angular scale ($\sim8°$ for the inner disk), required effective observing techniques and mosaicing methods and required the development of new deconvolution algorithms (Sault, Staveley-Smith, & Brouw 1996).

At the largest scales, understanding the interaction of the LMC with the Galaxy and the Small Magellanic Cloud (SMC) is important (Weinberg 2000). Also important is knowing the viewing geometry of the disk of the LMC (van der Marel & Cioni 2001), its mass and dark matter content (Kim et al. 1998a; Alves & Nelson 2000) and the origin of the off-center bar (Zhao & Evans 2000). At intermediate scales, the origin of the supergiant shells is tantalizing. Are supernovae and stellar winds (Chu & Mac Low 1990; Olsen et al. 2001; Tenorio-Tagle et al. 2003) sufficient, or are other factors such as instabilities in the ISM (Wada, Spaans, & Kim. 2000), high-velocity cloud collisions (Tenorio-Tagle & Bodenheimer 1980; Espresate, Cantó, & Franco 2002) or gamma ray bursts (Efremov, Elmegreen, & Hodge 1998; Efremov, Ehlerova, & Palous 1999) important? At smaller scales, the structure of the ISM, the structure of photo-dissociation regions and the detailed feeding and feedback of star-forming regions is important for understanding their

evolution. In §2, we introduce the method for linearly combining synthesis and single-dish observations and present the results. We describe Hα observations of the LMC in §3. We present H I supergiant shells in §4. A brief discussion of the paper is given in §5.

II. H I IMAGING

Several techniques are available to combine the interferometric and single-dish data. The data can be combined during a joint maximum entropy deconvolution operation. Alternatively the single-dish data can be used as a 'default' image in a maximum entropy deconvolution of the interferometer data. Another possibility is a to feather together (a linear merging process) the single-dish and interferometer images. The technique we have used is a variant of the approach described by Schwarz & Wakker (1991). As the Parkes and ATCA images give accurate representations of the LMC at short spacings and mid to long spacings respectively, a composite image can be formed by filtering out the short spacing data from the ATCA image, and then adding the Parkes image. This process is most easily visualized in the Fourier domain where it shows the expected amplitude as a function of spatial frequency of a point source for our observations. The Fourier transform of the Parkes images were added to the final images with no weighting (i.e. 'natural' weight in interferometric nomenclature). The deconvolved ATCA data was also Fourier-transformed, but by down-weighting the lower spatial frequencies such that the combined weight of the Parkes and ATCA data was the same as the response to a 1.'0 Gaussian. The MIRIAD task IMMERGE was used.

Before combining, the Parkes image was interpolated onto the same coordinate grid as the ATCA mosaicked image. Also the residual primary beam attenuation remaining in the ATCA image was applied to the Parkes image (the mosaicing process we have used does not perform full primary beam correction when this would result in excessive noise amplification). In order to perform the combination of the Parkes and ATCA observations, we need to ensure that the flux calibration between the two data types are consistent. Ideally we would like to find the ratio of the flux density of an unresolved point source in the field. We have estimated this calibration factor by examining data in the Fourier plane between 21 and 31 meters – data in this annulus is well measured by the Parkes and mosaicked ATCA observations. After tapering the ATCA data to the same resolution as the Parkes data, we found a scale factor of 1.3 minimized the L_1 difference between the interferometer and single-dish Fourier components (the real and imaginary parts of the data where treated as distinct measurements in the fitting). Note that the scale factor (and indeed the entire feathering process) requires a good estimate of the resolution of the Parkes image. The effective beam size of 16.9 arcmin was adopted as it gave a scale factor independent

of spatial frequencies. The resolution of the combined H I image of the LMC is 1.'0 which is the same as for the ATCA interferometer map. The RMS noise of the combined map, determined from the line-free parts of the final data cube, is ~19 mJy beam^{-1}. This corresponds to a brightness temperature sensitivity of ~ 3.2 K. We present the combined data set in the form of velocity channel maps in Figure 1. The other velocity channel maps, spatial-spatial map integrated over the full velocity range, and spatial-velocity maps at forty galactic longitude can be found in Kim et al. (2003).

III. Hα SURVEY

In order to compare the distribution of the unionized, but photo-dissociated gas traced by the H I with the distribution of ionized material (the H II regions) we undertook an imaging survey of the LMC in the Hα line. This was obtained with a focal reducing camera lens mounted on the 16-inch telescope at Siding Spring Observatory. The Hα images cover the same area as the H I survey with comparable spatial resolution, and so provide a unique probe of the detailed relationship between the ionized phase and atomic phase, at a resolution which is well-matched to the scale of the star formation regions. The objective of the Hα survey of the LMC was to obtain an Hα image covering the same region of sky as our H I survey.

The Hα survey of the LMC covers the same region of sky as our H I survey. Since the field is wide, the images had to be obtained with a small telescope. We therefore mounted a 153 mm $f/5.0$ camera lens on the mount of the 16 inch telescope at Siding Spring with a near-focal-plane filter assembly. The images were recorded with a thick Loral (2048 × 2048) CCD cooled close to liquid nitrogen temperatures. With this setup, each 15 μm pixel corresponds to 20.''63 on the sky, giving a total field size of 11.7° square. Thus both the spatial resolution and field coverage were well matched to the parameters of the H I survey. The Hα filter was centered at 6569 Å and had a FWHM of 15 Å in the convergent beam of the lens near field center.

However, due to beam-dependent broadening of the effective filter bandpass, there will be un-calibrated variations in sensitivity across the field. aswell as some contamination by the nearby [NII] lines at 6584 Å and 6548 Å . In addition to the Hα images, continuum images were taken through a filter centered at 6620 Å . Median-filtered sky flats were used for CCD calibration and cosmic ray has been removed by taking multiple exposures in each filter. The exposure time for both Hα and continuum images was 4 × 900 s. The four images of each filter were registered and shifted. Then those images taken through the same filter were combined using an average sigma-clipping algorithm by median. The continuum subtraction from the final Hα image was accomplished by scaling the continuum image so that the total star signal above the sky was the same as for the Hα image. The resulting Hα image of the
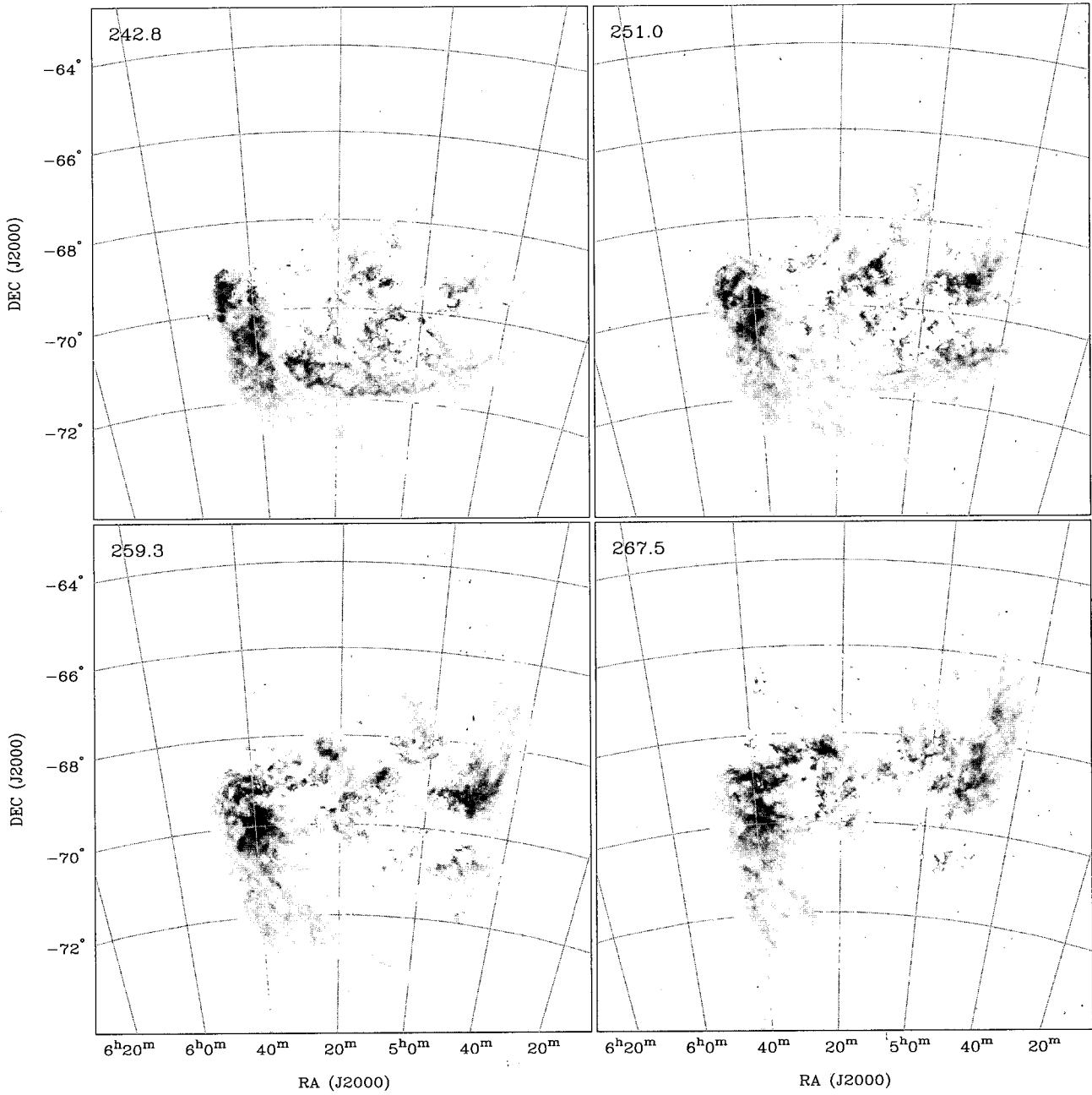
Fig. 1.— The individual channel maps for the H I datacube in the LMC. The heliocentric velocity is marked at the top left in each panel. Each panel is the average of five adjacent channels of width 1.649 km s^{-1} giving a panel spacing of 8.2 km s^{-1} . Black represents regions with the highest brightness temperatures of 136.7 K; white represents 0 K.

LMC is shown in Figure 1 of Kim et al. (1999). The Hα observations from this survey clearly resolve the Hα filaments, arcs, and ring-like structures in detail.

IV. H I SHELLS

The structure of the neutral atomic ISM in the LMC shows a complex distribution of H I emission, which is chaotic with hundreds of clouds, shells, arcs, rings, and filaments. The shell-like structures seen in the ATCA map still dominate the structure of the neutral atomic ISM in the LMC revealed by the ATCA+Parkes combined map. The previous visual survey of H I shell candidates chosen from the ATCA H I data cube (Kim et al. 1999) has been re-investigated from the current combined data set in Kim et al. (2003) and the physical parameters of the individual supergiant shells (Figure 2) are summarized in their Table 1. H I shells are H I regions confined within the main H I layer in the LMC. A simple rule of thumb would be to define such shells as having a radius less than the scale height of the H I gas in the LMC. In larger regions than this, the shape of the bubble will be very strongly modified by the density gradient, being flattened on the side nearest the galactic plane, and extended out of the plane. H I supergiant shells would then be those regions whose extent above the plane is so much larger than the H I scale height that the hot gas produced within the shell has broken out of the plane and is either draining out or has drained into the hot halo gas around the LMC. Such regions will have formed galactic chimneys which are perpendicular to the disk plane.

When a supergiant shell is drained of the overpressure which is driving the expansion of the H I shell, it has reached a momentum-conserving phase, and its expansion velocity in the galactic plane will reduce as more and more disk gas is swept up into the expanding H I shell. Unless it is powered by secondary star formation around its periphery, it will lose its identity either when the expansion velocity falls below the random turbulent velocity of the disk gas, or else when the differential velocity shear due to rotation becomes larger than the expansion velocity. This provides a simple and physically meaningful distinction between the various shell classes.

The age of each shell, t_s (in units of Myr), has been estimated from $t_s = 3R_s/5V_s$. Here R_s is the shell radius in units of pc and V_s is the expansion velocity of the shell in units of km s^{-1}. This equation is given by the standard theory of wind-driven bubbles (Weaver et al. 1977). The supergiant shells are much more likely to be in their momentum-conserving phase of evolution, in which case we have a different functional relation. If t_w is the age at which the bubble bursts out of the gas layer, for which the radius is R_w and the velocity of expansion is

$$t_s = t_w + \frac{R_s{}^4 - R_w{}^4}{4R_w{}^3 V_w} \qquad (1)$$

This is derived from the momentum-conserving equation of motion of the shell after break-out.

The velocity at break-out is given by

$$V_w = V_s \left(\frac{R_s}{R_w}\right)^3 \qquad (2)$$

from which, t_w the dynamical age of the shell at $R_w = 170$ pc, can be computed using the Weaver et al. (1977) equation (given above). The measured ages of these expanding supergiant shells are distributed between 3 Myr and 25 Myr (Kim et al. 1999, 2003). The ages of expanding giant shells can be calculated directly from Weaver et al. (1977) formula where their H I expansion velocities can be determined.

In general, the giant shells are younger than the mean age of the stars of the apparent OB association in the LMC. A demonstrative example of this is the superbubble in the N44 complex, where the dynamical time-scale of the bubble $3/5(r_s/v_s) = 1 - 2$ Myr (Meaburn & Laspias 1991; Kim et al. 1998b) is much less than the age of $\gtrsim 10$ Myr suggested by the H-R diagram for the interior stars of the OB association LH 47 (Oey & Massey 1995). Besides N44, many superbubbles exhibit expansion velocities that are too high to be consistent with the standard evolution, and a correlation of bright X-ray emission with many of these objects suggests acceleration by SNR impacts. It is interesting to note that the apparent age of shells in the LMC is similar to that in the SMC. By comparison, in the case of HoII, a galaxy with a similar mass and gas fraction to the SMC, the mean age of the shells is estimated to be much greater as 61 Myr and the youngest shells are 9 Myr (Puche et al. 1992). This may indicate that the recent star formation history in the LMC and SMC has been affected by their tidal interaction.

V. DISCUSSION

We find that total power data is important in recovering the true source structures even linear mosaicing technique recovers the 'missing' short spacings in the uv plane (Ekers & Rots 1979; Cornwell 1988). The structure of the neutral atomic ISM in the LMC reveals the clumpiness of the H I distribution over the whole of the LMC. Kim et al. (2003) have identified and catalogued H I clouds in the LMC by defining a cloud to be an object composed of all pixels in right ascension, declination, and velocity that are simply connected and that lie above the threshold brightness temperature. The power-law distribution of the size spectrum of H I clouds is similar to the typical size spectrum of the holes and shells in the H I distribution.

The diffuse interstellar clouds observed in the 21-cm H I line are mainly cooled by collisional excitation of the fine-structure levels of C$^+$ (Dalgarno & McCray 1972). In these regions, the C is ionized by the 11.2–13.6 eV part of the radiation field, and the C II fine structure
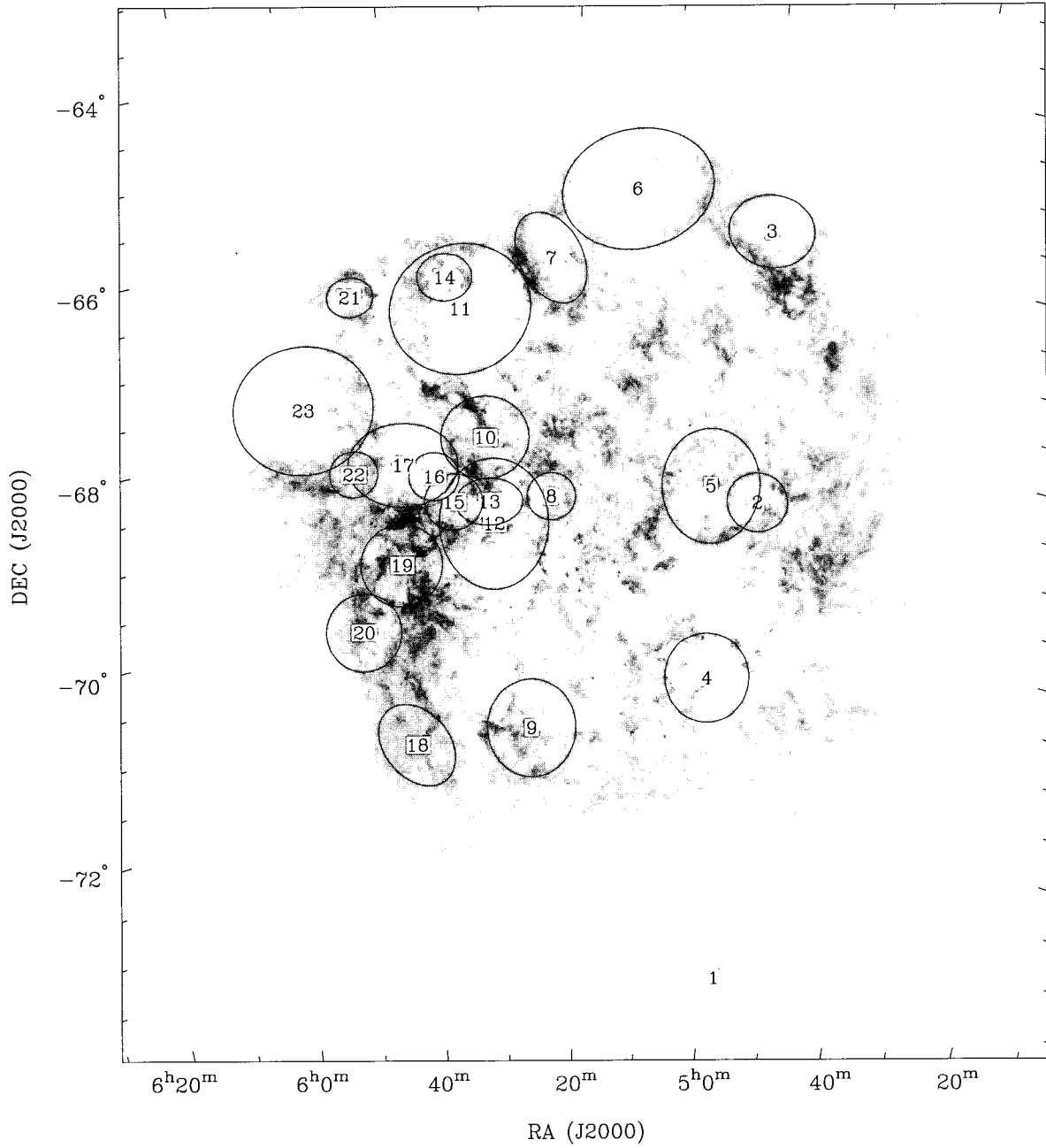
Fig. 2.— The spatial distribution of supergiant H I shells on the peak brightness H I map of the LMC.

lines are excited by collisions with H-atoms and electrons, as in the Milky Way. For the highest H I column densities (see Figure 3 in Kim & Reach 2002), the C II brightness increases more rapidly than the slope, Φ, obtained for the lower column density points. The excess C II emission for these points is plausibly due to formation of H_2, such that N(HI) is no longer a linear measure of the total H nucleon column density. However, the excess C II emission for these points could also be due to a higher radiation field due to massive stars forming in regions with higher column density.

ACKNOWLEDGEMENTS

REFERENCES

Alves, D.R., & Nelson, C.A. 2000, ApJ, 542, 789

Chu, Y.-H., & MacLow, M.-M. 1990, ApJ, 365, 510

Cornwell, T.J. 1988, A&A, 202, 316

Dalgarno, A., & McCray, R.A. 1972, ARA&A, 10,375

de Blok, W. J. G., McGaugh, S. S., Bosma, A., & Rubin, V. C. 2001, AJ, 552, L23

Dopita, M. A., Mathewson, D. S., & Ford, V. L. 1985, ApJ, 297, 599

Efremov, Y., Elmegreen, B.G., Hodge, P. 1998, ApJ, 501, 163

Efremov, Y. N., Ehlerová, S., & Palous , J. 1999, 350, 457

Espresate, J., Cantó, J., Franco, J. 2002, ApJ, 575, 194

Ekers, R.D., & Rots, A.H. 1979, in *Imaging Formation from Coherence Functions in Astronomy*, eds. van Schooneveld, C. (Dordrecht: Reidel), p.61

Feast, M.W. 1991, in *The Magellanic Clouds: Proceedings of the 148th Symposium of the International Astronomical Union*, eds. Haynes, R., & Milne, D. (Dordrecht: Reidel), p.1

Kim, S., Staveley-Smith, L., Dopita, M.A., Freeman, K.C., Sault, R.J., Kesteven, M.J., & McConnell, D. 1998a, ApJ, 503, 674

Kim, S., Chu, Y.-H., Staveley-Smith, L., & Smith, R. C. 1998b, 503, 729

Kim, S., Dopita, M.A., Staveley-Smith, L., & Bessell, M. 1999, AJ, 118, 2797

Kim, S., & Reach, W. 2002, ApJ, 571, 288

Kim, S., Staveley-Smith, L., Dopita, M. A., Sault, R. J., Freeman, K. C., Lee, Y., & Chu, Y.-H. 2003, ApJS, 148, 473

Luks, T., & Rohlfs, K. 1992, A&A, 263, 41

Meaburn, J., & Laspias, V.N. 1991, A&A, 245, 635

McGee, R.X., & Milton, J.A. 1966, Aust. J. Phys., 19, 343

Oey, M. S., & Massey, P. 1995, ApJ, 452, 210

Olling, R. P. 1996, AJ, 112, 481

Olsen, K.A.G., Kim, S., & Buss, J.F. 2001, AJ, 121, 3075

Puche, D., Westpfhal, D., Brinks, E., & Roy, J. 1992, AJ, 103, 1841.

Schwarz, U.J., Wakker, B.P. 1991, in *Radio Interferometry: Theory, Techniques and Applications*, Cornwell, T.J., Perley, R.A. eds. ASP Conf. Series, San Francisco, p. 188

Tenorio-Tagle, G., & Bodenheimer, P. 1980, ARA&A, 26, 145

Tenorio-Tagle, G., Palous, J., Silich, S., Medina-Tanco, G.A., Munoz-Tunön, C. 2003, A&A, 411, 397

Wada, K., Spaans, M., Kim, S. 2000, ApJ, 540, 797

Walter, F., & Brinks, E. 2001, AJ, 121, 3026

Weaver, R., McCray, R., Castor, J., Shapiro, P., & Moore, R. 1977, ApJ, 218, 377

Weinberg, M.D. 2000, ApJ, 532, 922

Westerlund, B.E., & Mathewson, D.S., 1966, MNRAS, 131, 371

van der Marel, R.P., & Cioni, M.L. 2000, AJ, 122, 1807

Zhao, H.S., & Evans, N.W. 2000, ApJ, 545, 35